Flexible/Branched Block Copolymer Melts

Galen T. Pickett

Department of Physics and Astronomy, California State University, Long Beach, 1250 Bellflower Boulevard, Long Beach, California 90840

Received August 28, 2001; Revised Manuscript Received December 4, 2001

ABSTRACT: I determined the phase boundaries for regularly branched block copolymers in the self-consistent classical path, circular/spherical unit cell approximation. In contrast to the case for linear chains, end-free "dead" zones are highly suppressed for highly branched molecules, greatly simplifying the integral equations to be solved. For the linear/branched diblock copolymers considered here, the phase boundaries between microphases are considerably shifted toward small volume fractions of the branched species. The equilibrium distribution of chain free ends is asymptotically uniform at high degrees of branching, consistent with the "filled core" picture of single dendrimer conformations.

1. Introduction

Hyperbranched molecules pose intriguing possibilities for control of interfacial properties,[1] especially as control over their synthesis and architecture has become breathtaking.[2−5] The dendrimer can have limbs of differing compositions or arms whose composition is a function of distance from the molecule center. The proliferation of chain tips, each of which can be decorated with an important functionality, is especially attractive for a range of practical applications. These molecules have the potentiality for complex single-molecule structure formation and, hence, specificity of *biological* interactions. Even in the absence of intrachain specific interactions, the dendritic arms are susceptible to demixing solely on the basis of their packing interactions.[6]

The application of interest here is controlling the microdomain morphology of linear−dendritic block copolymer melts. Ordinary multiblock copolymers are composed of long runs of same-type monomers (blocks) placed on a linear chain. The simplest such molecules forming interesting microdomains are the diblock copolymers,[7] where there are essentially two homopolymers (the first of type A monomers and the second of type B monomers) joined end-to end. At low temperature, demixing of A and B monomers occurs locally, but not globally, as a result of the irreversible chemical link between the blocks. As a function of the average composition of the chain and temperature, several microdomain textures appear spontaneously in thermal equilibrium. In the strongly segregated regime (low temperature, sharp interfaces between A- and B-rich domains), the microphases that appear are spherical domains either close packed or on a bcc lattice, passing to cylinders packed on a hexagonal lattice and then to lamellar domains where the A and B domains form alternating planes or material. These "classical" phases are the only possibilities in the asymptotic low-temperature limit, characterized by $\chi N \rightarrow \infty$, where N is the overall molecular weight of the copolymer, and χ is the Flory−Huggins interaction parameter between A and B monomers. For moderate χN, there are exotic gyroid and bicontinuous phases.[8]

Through a variety of mechanisms, this strong-segregation-limit phase diagram can be moderately shifted[9] and warped to suit some desired properties. By choosing the monomers to displace different volumes, or by making one block considerably stiffer than the other, the phase boundaries between the classical phases can be shifted. It has been suggested[10,11] that choosing one block to have a hyperbranched architecture allows major, sweeping shifts in the diblock phase diagram. Roughly speaking, even for a symmetric overall composition, the regular branchings of the B block (e.g.) will favor interfacial curvature forcing the B chains to splay outward, relieving some packing constraints. There has been predicted the interesting possibility that the diagrams can be shifted toward keeping an extreme minority branched species on the exterior of the domains.[11] As photonic band-gap devices are predicted for materials with sufficient index mismatch packed on a bcc lattice where the interstitial domains occupy a small volume fraction,[12,13] these dendritic molecules could find wide application.

These classical phases, "spherical", "cylindrical", and "lamellar" have close analogies to single-molecule dendrimer conformations. For example, spherical domains are structurally very similar to single dendrimer molecules, where several branches come together in a small region, and the dendritic arms splay outward. Cylindrical domains are quite similar to dendrimer comb molecules,[14,15] where hyperbranched chains are periodically grafted to a flexible backbone. The lamellar phase is likewise similar to the end-grafted "brush" layer.[16,17] What I look at here builds upon each of these pictures, allowing the size, and packing of flexible/dendrimer copolymers to adjust itself in thermodynamic equilibrium.

The theoretical approach that has been taken previously,[11] is the simplest one possible for strongly segregated systems, the famous Alexander−de Gennes approximation.[18,19] Here, all chain free ends are assumed to be localized along a single surface. Squelching the internal degrees of freedom of the chains greatly simplifies the theoretical development of block copolymer thermodynamics. This approximation maintains all the correct scaling laws for the single-chain free energy, and the microdomain length scales in the strongly segregated regime at a cost of overestimating the chain free energy by only about 20%, *at least for linear diblocks*. As applied to the conformation of single dendrimer molecules, this approximation, however, is essentially

10.1021/ma011532i CCC: $22.00
Published on Web 02/01/2002

the statement that all the dendritic tips are partitioned to the surface creating a "hollow-core" dendrimer.[20] As has been fairly well established, first in simulations[21,22] and other theoretical developments[23] and now more and more experimentally,[24] the tips of the dendritic molecule are strongly distributed throughout the conformation of the molecule ("filled core"). Thus, I can expect that the Alexander picture might be systematically troublesome for dendritic molecules, and I step past this approximation in the present note. Additionally, while my interest here is focused on strongly segregated copolymers, the single-chain scattering function for hyperbranched polymers derived in ref 23 could be used to calculate how ordering in the weakly segregated limit is affected by branching.

Indeed, a systematic improvement upon the Alexander picture has been available for diblocks for quite some time. The essential approximation involved is again a quashing of some of the chain degrees of freedom, in this case the suppression of all fluctuations around those chain conformations strictly minimizing the single-chain free energy.[25,26] This so-called "classical path" approximation correctly predicts a parabolic pressure for lamellar domains, as well as a parabolic composition profile for densely grafted linear homopolymers in good solvent. This parabolic pressure and profile incredibly survive when the end-grafted brush is composed of regularly branched dendrimers,[17] and I can expect that this parabolic behavior survives in copolymer domains, as indeed we see below. An interesting result of the tendency of dendrimers to distribute their free ends throughout space is that the existence of "dead" zones[25,27] (end-free zones required in linear brushes grafted to convex domains to avoid overfilling space) can be in general avoided. While dendrimer domains are inherently more complicated that their diblock copolymer analogues, the absence of the dead zone greatly simplifies their analysis.

The paper is organized as follows. I initially describe the classical path calculation and then the formalism of the numerical Scheutjens and Fleer[28] lattice calculations that will be compared to the classical path. Then, the phase diagrams for the linear/branched copolymer will be developed, and the comparison to that generated by the Alexander and the lattice numerical self-consistent field will be determined. Discussing the absence of the dead zones, and the remarkable inability of the Alexander model to correctly model these systems will be discussed, and then the conclusions will be offered.

2. Classical Path Model

The polymers in question have an A block consisting of a single, linear strand of N_A monomers, joined to a B block consisting of a regularly branched dendritic polymer of G generations, with monodisperse flexible spacers of molecular weight N_B, as in Figure 1. Thus, the G1 species is an ordinary diblock copolymer, with total molecular weight $N_A + N_B$, and the volume fraction of B monomers, ϕ, satisfys

$$\phi = N_B/(N_A + N_B) \tag{1}$$

In general, the total molecular weight of the chain is

$$N = N_A + N_B(2^G - 1) \tag{2}$$

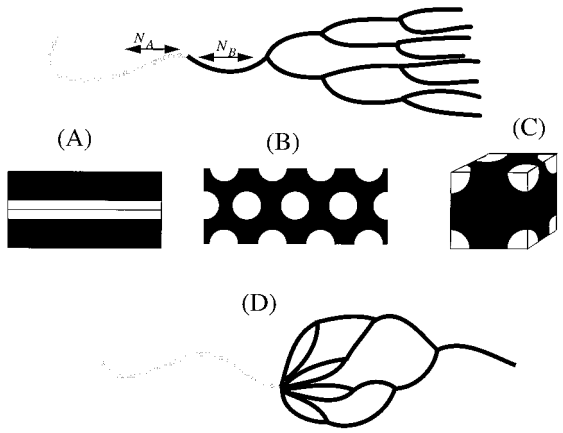

Figure 1. Schematic. Here, a G4 B block is grafted to a flexible A block. The ordering possibilities are (A) lamellar, (B) cylindrical, and (C) spherical. (D) Tip−graft AB copolymer, for which the Alexander−de Gennes model is essentially exact.

and the fraction of B monomers is given by

$$\phi = \frac{N_B(2^G - 1)}{N_A + N_B(2^G - 1)} \tag{3}$$

In the strong segregation limit, the phase boundaries between the lamellar, cylindrical, and spherical "classical" phases should be entirely a function of ϕ. The location of these phase boundaries, of course, will depend on the overall generation G of the B block. As in ref 11, I expect these phase boundaries to be shifted significantly toward keeping the branched block on the *exterior* of the curved microdomains. To determine these phase boundaries, I need to compare $F_{lam}(\phi, G)$ to $F_{cyl}(\phi, G)$ to $F_{sph}(\phi, G)$. In each case, the morphology with the lowest free energy per chain is the equilibrium phase.

Let us begin with the calculation for $F_{lam}(\phi, G)$. While the overall fraction of B monomers is fixed by the chemistry of the chain, eq 3, the overall *width* of the lamellar pattern is not. Let $h = h_A + h_B$ be the total width of a single lamellar half-layer (so that the bulk pattern has a total repeat spacing of $2h$). Let σ be the number of chains per unit area at the A−B interface. The fact that I consider meltlike conditions imposes two relationships between σ, ϕ, h, h_A, and h_B:

$$\phi = h_B/h \tag{4}$$

$$a^3N = h/\sigma \tag{5}$$

so that h_A and h_B can be written in terms of σ and ϕ:

$$h_A = (1 - \phi)Na^3\sigma \tag{6}$$

$$h_B = \phi Na^3\sigma \tag{7}$$

where a^3 is the volume a single monomer takes up in the melt (assumed to be the same for both A and B monomers).

To calculate $F_{lam}(\phi, G)$, I can independently calculate the free energy per A block, F_A, the free energy per B block, F_B, and the interfacial energy per chain, F_{surf}. Here, the A block forms a linear polymer brush, and its free energy has been calculated many times:[25,26]

$$F_A = \frac{\pi^2}{8}\frac{{h_A}^2}{N_A} = \frac{\pi^2}{8}(1-\phi)\sigma^2 N \tag{8}$$

Also, if the surface energy between A and B monomers is γ, then the surface energy per chain is simply

$$F_{surf} = \frac{\gamma}{\sigma} \tag{9}$$

All that remains is to calculate the free energy per branched block, a nontrivial task.

Let us start with an appropriate free-energy functional that can be used to determine both the configuration of these branched chains and F_B:

$$F_B[z(z_o, n)] = \int_0^{GN_B} f(n)\left[\frac{1}{2a^2}\left|\frac{dz}{dn}\right|^2 + P(z(z_o, n))\right] \tag{10}$$

Here, $z(z_o, n)$ is the *primitive* trajectory of the dendrimer block,[17] all of whose free ends are held at $z = z_o$ and whose single trunk chain is attached to the $z = 0$ plane where the A and B domains meet. The function $f(n)$ counts the number of statistically equivalent chain segments as a function of chemical index. Near the free ends ($0 < n < N_B$ in eq 10), there are 2^{G-1} equivalent chain segments. As shown schematically in Figure 1 for a G4 diblock

$$f(n) = 2^{G-1} \quad \text{when } 0 \le n < N_B \tag{11}$$

$$f(n) = 2^{G-2} \quad \text{when } N_B \le n < 2N_B \tag{12}$$

$$\vdots$$

$$f(n) = 1 \text{ when } (G-1)N_B \le n \le GN_B \tag{13}$$

The fact that each statistically identical chain segment follows exactly the *same trajectory* is true only in the classical limit, that is when Gaussian fluctuations of the chain trajectories around those minimizing $F_B[z(z_o, n)]$ are negligible.[17]

The free energy functional in eq 10 essentially states that each of the $f(n)$ equivalent strands have to be stretched a certain amount dz, and each of them needs to be inserted into the layer at the height $z(z_o, n)$ at the cost of $P(z)$ per monomer. When the B-block is an unbranched G1, then it is well-known that the potential $P(z)$ is uniquely determined by the monodispersity of the chains. In the language of classical mechanics, a particle dropped the height z_o from rest hits the "ground" in a "time" N_B regardless of the initial position of the particle, z_o. The required potential has a parabolic form:

$$P(z) = P_o(h^2 - z^2) \tag{14}$$

The required equal-time potential is *harmonic*. Since the total transit time of the classical particle is known to be one-quarter of the full oscillation period of this equivalent oscillator, I must have[26]

$$P_o \equiv \frac{{\omega_o}^2}{2a^2{N_B}^2} \rightarrow \omega_o = \frac{\pi}{2} \tag{15}$$

When the chain is regularly branched, with statistically identical segments, I can retain the form for the insertion potential per monomer as in eq 14, but with a different expression for P_o and ω_G.[17] Minimizing eq 10 with respect to variations in $z(z_o, n)$ yields the Euler–Lagrange equation of motion:

$$\frac{d}{dn}\left(\frac{f(n)}{a^2}\frac{dz}{dn}\right) = f(n)\frac{d}{dz}P(z) \tag{16}$$

With the ansatz, shown in eq 14, and the definition of P_o given in eq 15, this becomes:

$$\frac{d}{dn}\left(\frac{f(n)}{a^2}\frac{dz}{dn}\right) = -f(n)\frac{{\omega_G}^2}{a^2{N_B}^2}z(z_o, n) \tag{17}$$

When the chemical index is not an integral multiple of N_B, the factor $f(n)$ is a constant, and the equation of motion during these times is

$$\frac{d^2}{dn^2}z(z_o, n) = -\frac{{\omega_G}^2}{{N_B}^2}z(z_o, n) \tag{18}$$

Thus, the trajectory must be a continuous piecewise harmonic function. When the chemical index is an integral multiple of N_B, the weighting function $f(n)$ is cut discontinuously in half. Integrating the equation of motion from just below this discontinuity to just above it yields a boundary condition pasting together the harmonic pieces of the overall trajectory:

$$2\frac{dz}{dn}|_{gN_B^-} + \frac{dz}{dn}|_{gN_B^+} \quad \text{for each } g = 1 \ldots g = G \tag{19}$$

Thus, the *velocity* along the chain doubles at the junction points to make up for the fact that half of the chains entering the junction terminate there.

If I label the G harmonic pieces of the trajectory so that

$$z(z_o, n) = z_o z_1(n) \quad \text{for } 0 \le n < N_B \tag{20}$$

$$z(z_o, n) = z_o z_2(n) \quad \text{for } 0 \le n < 2N_B \tag{21}$$

$$\vdots$$

$$z(z_o, n) = z_o z_G(n) \quad \text{for } (G-1)N_B \le n \le 2GN_B \tag{22}$$

then I can write each of the harmonic pieces of trajectory as

$$z_g = A_g \cos\frac{n\omega_G}{N_B} + B_g \sin\frac{n\omega_G}{N_B} \tag{23}$$

The initial conditions on the trajectory ($z(z_o, 0) = z_o$, and $dz/dn|_{n=0} = 0$) thus determine the constants A_1 and B_1:

$$A_1 = 1 \quad \text{and} \quad B_1 = 0 \tag{24}$$

Continuity of the trajectory is ensured by $z_g(gN_B) = z_{g+1}(gN_B)$ or

$$A_g \cos\omega_G g + B_g \sin\omega_G g = A_{g+1}\cos\omega_G g + B_{g+1}\sin\omega_G g \tag{25}$$

The condition of mechanical equilibrium at the junction points, eq 19, is enforced when

$$2(-A_g \sin \omega_G g + B_g \cos \omega_G g) = (-A_{g+1} \sin \omega_G g + B_{g+1} \cos \omega_G g) \quad (26)$$

This set of $2G$ equations can be easily solved numerically. To determine the solution completely requires the determination of ω_G, by requiring that

$$z_G(z_o, GN_B) = 0 \quad (27)$$

that is, that the trajectory arrives at the A/B junction plane using up exactly the correct number of B monomers. Equation 27 is generally a $G - 1$ polynomial in $\cos \omega_G$. There are undoubtedly multiple roots of this equation. The appropriate root to take, however, is the one for which the *entire trajectory* takes place for $z > 0$. This condition is enough to uniquely determine ω_G, and in Table 1, I show the values of ω_G that are used in this paper. Furthermore, Figure 2 shows the piecewise harmonic trajectories for several generations.

With the trajectories thus determined, the free energy per B block can be determined subject to the constraint that the dendrimer block has all of its free ends located at z_o, simply by using the known trajectory in eq 10. Since each of the A_g, $B_g \sim z_o$, the following scaling holds:

$$F(z_o) = \frac{{z_o}^2 {\omega_G}^2}{2N_B} \sum_g \int_{g-1}^{g} dm\, (-A_g \sin \omega_G m + B_g \cos \omega_G m)^2 f(mN_B) - \frac{{z_o}^2 {\omega_G}^2}{2N_B} \sum_g \int_{g-1}^{g} dm\, (A_g \cos \omega_G m + B_g \sin \omega_G m)^2 f(mN_B) + \frac{{z_o}^2 {\omega_G}^2}{2N_B} \int_0^G dm\, f(nN_B) \quad (28)$$

or after some rearranging

$$F(z_o) = \frac{{h_B}^2 {\omega_G}^2}{2N_B} \sum_g f(gN_B) \left(1 + \frac{{z_o}^2}{2{h_B}^2 \omega_G} T_g\right) \quad (29)$$

where T_g is given by

$$T_g = 2A_g B_g (\cos 2g\omega_G - \cos 2(g-1)\omega_G) + ({A_g}^2 - {B_g}^2)(\sin 2(g-1)\omega_G - \sin 2g\omega_G) \quad (30)$$

Clearly, when $G = 1$, so that $\omega_G = \pi/2$ and $A_1 = 1$, $B_1 = 0$, the free energy per B block is independent of z_o. This feature is lost for all other $G \neq 1$. Therefore, to calculate the average value of $F_B(z_o)$, I must determine the distribution of chain ends. The number of dendrimer chains with free ends in the region $(z, z + d_z)$ is given by $\xi(z)\, dz$, and $\xi(z)$ must be calculated. Once this is accomplished, the branched free energy per chain is given by

$$F_B = \int_0^{h_B} dz_o\, F_B(z_o) \xi(z_o) \equiv \frac{h^2}{N} f_B(G) \quad (31)$$

where the dimensionless B-chain free energy has been defined as $f_B(G)$. With eqs 8 and 9, eq 31 gives the free energy per chain for the lamellar phase, F_{lam}.

Determining $\xi(z)$ must proceed essentially numerically, although the general approach is the same as for the G1 lamellar domains. Given that the free ends of the branched chain are held at z_o, the volume fraction at the height z_1 taken up by monomers on this chain is given by

$$\phi(z_1, z_o) = \frac{f(n(z_o, z))}{dz/dn(z_o, n(z_o, z_1))} \quad (32)$$

where it is understood that $n(z_o, z)$ is the chemical index such that the trajectory calculated in eq 23 satisfies

$$z(z_o, n(z_o, z_1)) = z_1 \quad (33)$$

The factor of $f(n(z_o, z))$ in the numerator counts the fact that there are multiple, identical chain segments contributing to the partial volume fraction. For G1 copolymers, there is an analytic expression for $n(z_o, z_1)$, but in general this is strictly a numerical procedure. One must arrange $\xi(z_o)$ so that the B domain is completely filled with B monomers:

$$\sigma = \int_z^h dz_0 \xi(z_o) \phi(z_o, z) \quad (34)$$

Thus, $\xi(z_o)$ is normalized so that σ chains per unit grafting area are found in the layer. Equation 34 states that free ends can be distributed from the top of the grafted layer inward, at each height z_o by placing just enough chains to take up whatever empty space remains there. As long as $\phi(z, z_o)$ is a monotonically increasing

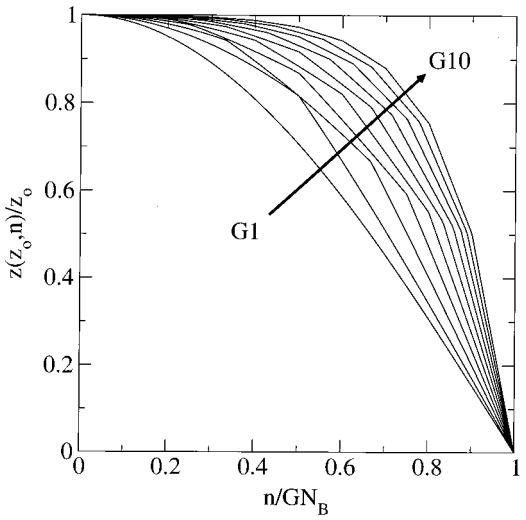

Figure 2. Classical path trajectories. Here, are shown the scaled trajectories for G1−G10, $z(z_o, n)/z_o$. The trajectories flatten considerably at high G and at small n, indicating that most of the monomers on the chain reside near the free end. The ansatz in eq 60 corresponds to $z(z_o, n)/z_o = 1$.

Table 1. Classical Path Dimensionless Frequency, ω_G, and Ratio of Alexander to Classical Energies for a Flat Brush

G	$\cos^2 \omega_G$	$G\omega_G$	$F_{Alexander}/F_{classical}$
1	0	1.570 796 326	1.215
2	$^2/_3$	1.230 959 417	2.639
3	$^8/_9$	1.019 510 728	5.527
4	$^1/_9(5 + \sqrt{13})$	0.843 642 816	11.68
5	$^2/_3(1 + \sqrt{^2/_3})$	0. 692 568 421	24.57
6	0.991 223 044	0.562 929 619	51.06
7	0.995 820 956	0.452 834 431	104.8
8	0.997 969 692	0.360 593 573	213.4
9	0.999 001 701	0.284 410 097	432.7
10	0.999 505 639	0.222 360 504	868.4

function of z, this can be accomplished with a unique nonnegative $\xi(z_o)$.

With $\xi(z_o)$ determined, the entire free energy per chain can be written as

$$F_{tot} = F_A + F_B + F_{surf} \tag{35}$$

or equivalently

$$F_{tot} = \sigma^2 N(\pi^2 8(1-\phi) + \phi f_B(G)) + \gamma\sigma \tag{36}$$

The unknown parameter is σ, which takes its equilibrium value when $dF_{tot}/d\sigma = 0$:

$$\sigma_{eq} = \left(\frac{2\gamma}{\frac{\pi^2}{8}(1-\phi) + \phi f_B(G)}\right)^{1/3} \tag{37}$$

The equilibrium free energy per chain in the lamellar phase is therefore

$$F_{lam} = \gamma^{2/3} N^{1/3} \frac{3}{2^{2/3}}\left(\frac{\pi^2}{8}(1-\phi) + \phi f_B(G)\right)^{1/3} \tag{38}$$

Again, it must be stressed that f_B must be determined numerically in the event that $G \neq 1$. The fact that the free energy scales as $\gamma^{2/3}N^{1/3}$ is preserved from the G1 diblocks, but in general the "prefactor" is a simple function of volume fraction, ϕ, and a rather complicated function of generation number G. As in the discussion below, this scaling with N and γ is preserved in the Alexander−de Gennes formulation of the dendrimer copolymer free energy. However, insisting that all free ends of the branched chains exist at the extreme tips of the B domains results in a spectacular overestimation of the chain free energy, especially at large G. Even still, the classical treatment and the Alexander−de Gennes treatment give remarkably similar phase diagrams.

To calculate the free energies of the cylindrical and spherical phases, only minor changes are needed. The relationship between volume fraction and h_A, h_B depends on dimension:

$$1 - \phi = \left|\frac{h_A}{h}\right|^2 \quad \text{for cylinders} \tag{39}$$

$$1 - \phi = \left|\frac{h_A}{h}\right|^3 \quad \text{for spheres} \tag{40}$$

Evidently, h_A and h_B can be written in terms of σ, ϕ, and N as

$$h_A = 2(1-\phi)Na^3\sigma \tag{41}$$

$$h_B = 2(\sqrt{1-\phi} - 1 + \phi)Na^3\sigma \quad \text{for cylinders} \tag{42}$$

and

$$h_A = 3(1-\phi)Na^3\sigma \tag{43}$$

$$h_B = 3((1-\phi)^{2/3} - 1 + \phi)Na^3\sigma \quad \text{for spheres} \tag{44}$$

Additionally, the free ends must be distributed according to a different law than that given in eq 34. For cylinders, I must have

$$(h_A + r)\sigma = \int_r^{h_B} dr_o\, \xi(r_o)(h_A + r_o)\phi(r_o, r) \tag{45}$$

For spherical domains, the relation is

$$(h_A + r)^2\sigma = \int_r^{h_B} dr_o\, \xi(r_o)(h_A + r_o)^2\phi(r_o, r) \tag{46}$$

After calculating $\xi(z_o)$ by inverting these integral relations numerically, I must check explicitly that $\xi(z_o)$ is strictly positive; that is, it has no "dead zones" or unphysical requirements that *negative* ends have to be distributed. With linear chains, it is well-known that such dead zones exist for any convexly curved substrate.[25,27] What is surprising (but is really only a straightforward consequence of the fact that dendrimers carry almost all of their molecular weight at their "tips" as in Figure 2) is that these dead zones are completely suppressed at a G-dependent curvature. In what follows below, I am careful to remark when this is violated. The suppression of the dead zone is essentially a consequence of the "filled core" property of single dendrimer molecules.[21−24]

3. Lattice SCF Model

To explicitly check the predictions of the classical path analysis, numerical self-consistent field methods must be employed,[8,29] and I choose to do so with the lattice self-consistent field method of Scheutjens and Fleer.[28] As above, there are N_A A-type monomers grafted to a dendrimer of type B monomers. The dendritic block of the copolymer consists of G generations, each arm consisting of N_B monomers. The total molecular weight of the copolymer is N, and there are G generations on the B block. Space is entirely filled in this lattice calculation with a combination of A and B monomers (each taking up an equal volume consisting of a single lattice site). Thus, I am examining the *incompressible melt* state of the neat copolymer liquid.

Given, $P_i(z)$, the free energy cost per i type monomer for insertion at the position z in the lattice, the statistics of a single dendrimer can be determined. First, I define the Boltzmann weight associated with P_i

$$g^i(z) = \exp[-P_i(z)] \tag{47}$$

where the energy scale is explicitly taken to be the thermal scale, $kT \equiv 1$. Let $\mathcal{G}_1^i(z)$ be the total statistical weight associated with a linear chain of N_i type-i monomers with one end located at z, in the given potential field $P_i(z)$. This weight can be built up through the recursion relations:

$$G^i(z, z';1, 1) = g_i(z)\delta_{z,z'}$$

$$G^i(z, z';1, n) = \langle G^i(z, z';1, n-1)\rangle g^i(z)$$

$$\mathcal{G}_1^i(z) = \sum_{z'} G^i(z, z';1, N_i) \tag{48}$$

where $G^i(z, z';1, n)$ is the statistical "propagator", or unnormalized statistical weight, of a linear chain segment of n monomers of type i proceeding from z to z'. Here, the angled brackets indicate a sum over nearest-neighbor lattice sites

$$\langle g^i(z)\rangle = \lambda_1(z)g^i(z-1) + \lambda_0(z)g^i(z) + \lambda_2(z)g^i(z+1) \tag{49}$$

for example, where $\lambda_1 = \lambda_2 = {}^1/_6$ and $\lambda_0 = {}^2/_3$ accounts for the fraction of nearest neighbor sites (on a simple cubic lattice with a total of six nearest neighbors). With the statistical weight $\mathcal{G}^{\mathrm{i}}_1(z)$, the full statistical weight attributed to the dendrimer copolymer can be determined. I define

$$\mathcal{G}^{\mathrm{i}}_M(z) = \sum_{z'} G^{\mathrm{i}}(z, z';1, N_i)\langle \mathcal{G}^{\mathrm{i}}_{M-1}(z')\rangle \qquad (50)$$

That is, $\mathcal{G}^{\mathrm{i}}_2(z)$ is the total weight associated with a strand of N_{i} monomers of type i beginning at z, proceeding to any z' where it is met by two strands of length N_{i}. Clearly, the entire weight associated with this copolymer is

$$\text{weight} = \sum_z \mathcal{G}^{\mathrm{A}}_1(z)\langle \mathcal{G}^{\mathrm{B}}_G(z)\rangle \qquad (51)$$

Thus, the Boltzman-weighted statistical sum for a single copolymer is made up of the weight of the A-strand meeting a G-generation B dendrimer at the position z in the lattice, summed over all positions in the lattice.

Given all of the $\mathcal{G}^{\mathrm{i}}_M(z)$, all relevant statistical averages can be made. In particular, the volume fraction due to the sth monomer on one of the two of the principle branches of the dendrimer block can be calculated as

$$\phi_{\mathrm{s}}(z) = \sum_{z_{\mathrm{o}},z_1,z_2} [\mathcal{G}^{\mathrm{A}}_1(z_{\mathrm{o}})\langle G^{\mathrm{B}}(z_{\mathrm{o}}, z_1;1, N)\rangle \times \langle \mathcal{G}^{\mathrm{B}}_{G-1}(z_1)\rangle G^{\mathrm{B}}(z_1, z;1, s) G^{\mathrm{B}}(z, z_2;s, N)\langle \mathcal{G}^{\mathrm{B}}_{G-2}(z_2)\rangle^2]/[\text{weight}(z_{\mathrm{o}})g(z)] \qquad (52)$$

where the additional factor of $g(z)$ in the denominator cancels out the double weighting of the s monomer taken by the two factors of G^{B} in the numerator. Thus, given $P^{\mathrm{A}}(z)$ and $P^{\mathrm{B}}(z)$, all of the statistics of the copolymer domain can be calculated. In particular

$$\phi_{\mathrm{tot}}(z) = \phi_{\mathrm{A}}(z) + \phi_{\mathrm{B}}(z) \qquad (53)$$

can be calculated. Self-consistency is enforced on $P^{\mathrm{i}}(z)$ when $\phi_{\mathrm{tot}}(z) = 1$, and

$$P^{\mathrm{A}}(z) = \alpha(z) + \chi\langle\phi_{\mathrm{B}}(z)\rangle \qquad (54)$$

$$P^{\mathrm{B}}(z) = \alpha(z) + \chi\langle\phi_{\mathrm{A}}(z)\rangle \qquad (55)$$

Here, $\alpha(z)$ is a "hard-core" potential, which must be chosen the same for A and B type monomers, and χ is the Flory−Huggins interaction parameter between A and B type monomers. The incompressibility constraint and self-consistency represents $2L$ highly nonlinear equations in the $2L$ unknown values of $P^{\mathrm{A}}(z)$, $P^{\mathrm{B}}(z)$ where L is the total size of the lattice. The required values of the potentials are determined through standard numerical methods.[28,30] When self-consistent values of the potentials have been determined, the free energy of the resulting conformation can be calculated as

$$F = \sum_z \log(\text{weight}(z)) + \frac{1}{2}\sum_{\mathrm{ij}} \chi_{\mathrm{ij}}\phi_{\mathrm{i}}(z)\langle\phi_{\mathrm{j}}(z)\rangle \qquad (56)$$

Here, $\chi_{\mathrm{ij}} = \chi\delta_{\mathrm{ij}}$ is the Flory−Huggins interaction parameter between monomer type i and monomer type j.

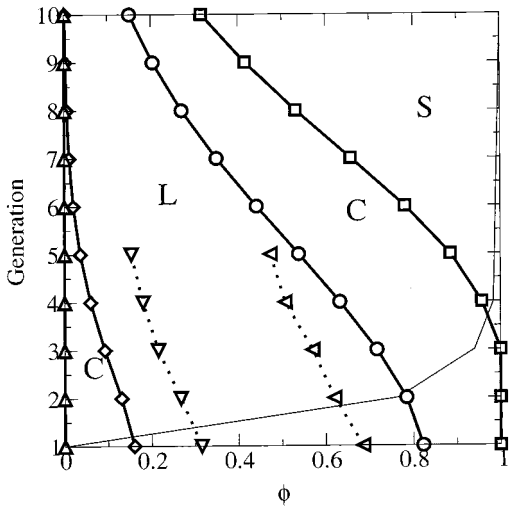

Figure 3. Phase diagram, classical path approximation. The phases are as marked on the diagram. In all cases, the phase boundaries are considerably shifted toward keeping the hyperbranched B block on the convex side of the AB interface. Also, up to G5, the phase boundary for lamellar−cylindrical transitions for $\chi = 0.5$, and the total number of B monomers on the chain equal to 64 (ϕ being determined by the total number of A and B monomers on each chain). Thus, χN ranges from 24 up to 96 for the most extreme asymmetries considered. These values of χN ensure that the calculations are uniformly situated in the strongly segregated regime. The shaded region is the region for which *negative* end-densities are required by the parabolic potential. Thus, the calculation in this region cannot be trusted. Dashed lines are the result of a two-dimensional lattice SCF calculation showing the transition line between the cylindrical and lamellar phases.

Thus, in various geometries, the free energies of the lamellar, cylindrical, and spherical phases can be determined.

The calculations have been carried out on a two-dimensional lattice, so that three-dimensional structures with one degree of translational invariance have been modeled. Thus, the calculations are restricted to determining the phase boundaries between the lamellar and cylindrical domains, but the Wigner−Seitz cell containing a single cylindrical domain is not circular in cross section. The packing of the cylinders on a hexagonal lattice relaxes this necessary approximation of the classical path analysis.

4. Results

In Figure 3, I have the phase diagram, in the strongly segregated regime, of these flexible-hyperbranched copolymers. The classical path calculations have been executed for G1−G10, and the lamellar (L), cylindrical (C), and spherical (S) phases have been compared. The solid lines indicate phase boundaries as calculated with the classical path. The lamellar phase is dramatically shifted toward low ϕ (that is, even a small amount of B on the chain is enough to stabilize the lamellar phase). The most dramatic shift occurs for the lamellar−cylinder transition in which the dendrimer occupies the interior of the cylindrical domains (the ◇ symbols in Figure 3). Interestingly, the *spherical phases* are pushed entirely off the phase diagram and either stay there (dendrimer interior to the spherical domains), or enter the phase diagram only at relatively high generation number (G4). This hardly matches the known strongly segregated behavior of the G1 copolymers (ordinary diblock copolymers), and is a symptom of the presence

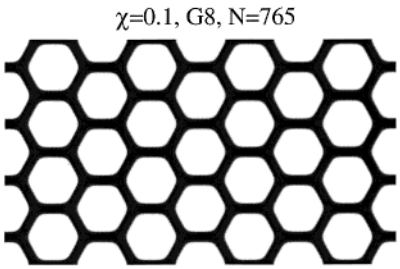

Figure 4. SCF profile for G8 dendrimers. The dendritic polymers occupy the darkly shaded regions. This example has $\phi = {}^1/_3$. The cylinders are substantially distorted, so that the "round/spherical" unit cell approximation must be abandoned.

of "dead" zones in the calculations for $G < 4$ and of the spherical unit cell approximation that has been used to calculate the classical path free energy.

The boundaries at low ϕ have the dendritic arms inside the cylindrical domains, and the flexible A blocks are on the exterior of the domains. The exterior A blocks *must exhibit* dead zones. In all cases, I have assumed that these A blocks, when confined to the exterior of the domains, are modeled satisfactorily by the Alexander−de Gennes picture. For linear chains, this introduces a free energy cost that is larger by a factor of approximately 1.2 than necessary (for flat domains) and is much more satisfactory than the huge overestimate made at higher values of G (see discussion, below, and Table 1).

The shaded region in Figure 3 indicates those regions in which the density of ends, $\xi(z_o)$ as calculated via eqs 45 and 46, becomes negative. This signals a breakdown in the parabolic ansatz for the monomer insertion potential, eq 14. A new self-consistent potential can be calculated, and a reliable estimate for the classical-path with dead zone free energy can be made, but this goes past the scope of the present development.[27]

The spherical/cylindrical unit cell approximation can be addressed with the lattice SCF model. Here, the calculations have been executed in two spatial dimensions, so that lamellae and cylinders can be faithfully represented. Spherical domains require a full calculation in three dimensions, at present too expensive for a site-by-site calculation on a three-dimensional simple cubic lattice, although such calculations have met success in a dual space of orthogonal functions of the required symmetry.[8] In any case, the dashed lines show the calculated phase boundaries between lamellar and hexagonally packed cylindrical domains for a variety of dendrimer-flexible copolymers. For all of these calculations, $\chi = 0.5$, and the number of B monomers on the chain has been set to 64. The number of A monomers has been adjusted to attain a desired value of ϕ, ranging from 32 to 128, so that χN varies from a low of 24 up to a maximum of 96. In all cases, these values lie in the strongly segregated regime.

The lamellar phase is drawn away from the extremes of the circular/spherical unit domain approximation, but still tilt severely off toward small ϕ. A typical configuration for G8 dendrimer is shown in Figure 4. Here, $N_B = 1$, so that there are $2^8 - 1 = 255$ monomers on the branched chain, and there are $N_A = 510$ monomers on the A chain so that $\phi = {}^1/_3$. While it was not possible to determine the phase boundaries at this high a generation number, this configuration does represent a local minimum in the free energy, and thus, it is a configuration accessible in a real experiment. The dark domains show the highest density of the dendritic arms, and the white domains show the greatest density of the flexible A chains. The A chains are confined to the interior of highly distorted cylindrical domains, and the B chains are confined to essentially flat domains with a convex curvature concentrated at the hexagonal vertexes. Thus, the free energy of the cylindrical domains is lowered toward that of the lamellar domains, resulting in an earlier lamellar−cylindrical transition that that predicted in the cylindrical unit cell model. While the classical path approximation tends to overestimate the effect that hyperbranching has on the shift in phase lines, it gives quite good qualitative agreement with the less restrictive lattice SCF calculations.

5. Discussion

The phase shifts predicted on the basis of the Alexander−de Gennes approximation[11] also give good qualitative agreement with the lattice SCF calculations, and at first glance it could seem that this is the usual case of a convenient approximation facilitating a nearly analytic calculation. Relaxing the convenient assumption leads to quantitatively, although not particularly qualitatively, more accurate results, at a cost of considerably more analytic and/or numerical effort. However, there are great differences between the Alexander−de Gennes picture and the classical path picture for dendrimer copolymers. In particular, while the free energy per branched block in both schemes scales as $\sigma^2 N$, the prefactor is generation dependent, and grows *exponentially* as G is increased. For G10 dendrimers, the free energy estimated in the Alexander model is a factor of 1000 larger than than given by the classical path picture.

To make the comparison, I follow the analysis of ref 11, estimating the free energy per branched block in the Alexander picture. Here, I assume that all of the dendrimer free ends lay at the same distance from the AB interface in each of the flat, cylindrical, and spherical domains. In each case, the free energy of the A blocks is the same, regardless of geometry

$$F_A = \frac{h_A{}^2}{N_A}\frac{\pi^2}{8} \tag{57}$$

taking a slightly improved estimate over Semenov's for the free energy per chain grafted to a convexly curved surface. The change comes about when considering the B blocks, dendrimers grafted to either a flat surface (lamellar), cylindrical surface, or a spherical surface. In each case, it is necessary to estimate not only the stretching energy per chain, but the required insertion potential, P, capable of maintaining the chains with their ends localized. For a linear brush at a coverage of σ chains per unit area, the necessary potential is

$$\begin{aligned} P(z) &= \sigma^2 \quad \text{when } z < h \\ &= 0 \quad \text{otherwise} \end{aligned} \tag{58}$$

Each free end of this layer executes a discontinuous change in its degree of extension from a constant level of $dz/dn = h/N = \sigma$ to being unstretched right at the edge of the brush. This discontinuity in the rate of extension can only be maintained through a discontinuous change in $P(z)$, as above. When the chain is regularly branched, like a dendrimer, the potential has

many discontinuities in it, which must be calculated to determine the free energy of the chain. For a molten dendrimer brush at a coverage σ, the degree of local stretching can be determined simply from demanding that space be filled. Essentially, this breaks the dendrimer brush up into G linear brushes, all connected end-to-end. The "height" of the outermost such subbrush (containing the free ends of the dendrimers) is determined by $h_G = 2^{G-1}\sigma N$. This brush looks like an extremely crowded brush of N_B-molecular weight chains packed in at a grafting density of $2^G\sigma$. The final subbrush can be thought of as a brush of N-molecular weight chains, at the initial coverage, so that $h_1 = \sigma N$. Thus, the chain trajectory that is required has the chains *most stretched* far away from the grafting surface and least stretched *at the grafting surface*. Thus, the dendrimers are stretched the most where they keep most of their monomers, in stark contrast to the end-distributed, classical path model in Figure 2. There, the dendrimers are most stretched near their trunks, and are in fact asymptotically unstretched near their free tips. Thus, one can expect the Alexander−de Gennes picture for these dendrimer layers to overestimate free energies wildly.

The end-distribution in the Alexander picture is simple enough:

$$\xi(z_o) = \sigma\delta(h_B - z) \tag{59}$$

The fact that almost all of the molecular weight on the chain is carried at the tips for the classical path analysis gives an equally simple expression. Using the approximation

$$\phi(z; z_o) = \delta(z - z_o) \tag{60}$$

gives when inserted into eq 34

$$\xi(z_o) = \frac{\sigma}{h_B} \tag{61}$$

That is, ends are distributed *uniformly* in the asymptotic high G, flat limit. This fact ($\xi(z_o)$ = constant) is preserved in the cylindrical and spherical geometries as well. The asymptotic form for even G5 dendrimers (flat) are obeyed amazingly well.[17]

The free energy of the grafted Alexander dendrimer can be easily estimated, as by ref 11. Here

$$F_{\text{dendrimer}} = \frac{3\sigma^2 N}{14}\frac{2^{3G} - 1}{(2^G - 1)^2} \tag{62}$$

The Alexander free energy in eq 62 has been compared to the free energy calculated in the classical path analysis, and the ratio has been plotted in Figure 5. The overestimate is *extreme* for high G (a factor on the order of 1000 for G10 dendrimers), although naturally both results scale in the same manner with the arm molecular weight, N_B, and the surface coverage σ. Also plotted are the results of the Alexander approximation when the dendritic brush is grafted to the exterior of a cylindrical and spherical domain, such that the radius of the substrate is equal to the layer thickness of the grafted layer. For each of these moderate curvature cases, the Alexander model drastically overestimates the chain free energy, and thus the Alexander model has to be applied very carefully.

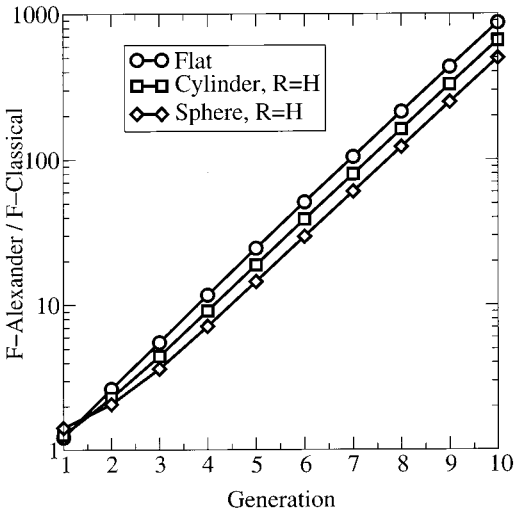

Figure 5. Comparison: Alexander−de Gennes and classical SCF. The free energies in both the Alexander−de Gennes and the classical path approximations are calculated and their ratio is reported in various geometries. The overestimate of the dendrimer free energy grows exponentially in generation number, G, getting as large as 10^3 for G10 dendrimers.

Essentially, the Alexander picture so overestimates the magnitude of the B-block free energy, that the A-block free energy is quite irrelevant at high G. Thus, it is not surprising that the Alexander picture fundamentally mischaracterizes the organization of the branched blocks but does an equally bad job in the lamellar, cylindrical, and spherical phases. Luckily, fair predictions for the microphase boundaries are possible. There is, however, a species of hyperbranched copolymers for which the Alexander picture is essentially *exact*. These are shown schematically in Figure 1D Here, all of the B free ends are gathered together and are joined to the A block. This "tip−graft" copolymer, while exceedingly complex to synthesize, will force the grafted blocks to organize themselves with the hyper-branched tips most strongly stretched, and the free ends least stretched. There should be a strong segregation of B-type ends, and virtually all the stretching free energy will be localized in the B blocks.

6. Conclusion

The flexible-dendrimer copolymer phase diagram has been calculated in the classical path approximation, and compares favorably to a numerical calculation with the lattice SCF theory of Scheutjens and Fleer. While the Alexander−de Gennes picture of these copolymer domains also gives a qualitatively correct phase diagram, that model seriously overestimates the stretching energy of the dendrimer molecules. The packing of free ends in the dendrimer is asymptotically *uniform* (at least as easy an approximation to handle as the Alexander picture), although tip−graft dendrimer copolymers should behave essentially as predicted by the Alexander model. As previously predicted, the hyperbranching of one of the species is sufficient to dramatically swing the microphase diagram toward low values of branched volume fraction.

References and Notes

(1) Voegtle, F.; Gestermann, S.; Hesse, R.; Schwierz, H.; Windisch, B. *Prog. Polym. Sci.* **2000**, *25*, 987.
(2) Ariga, K.; Urakawa, T.; Michiue A.; Sasaki, Y.; Kikuchi, J.-I. *Langmuir* **2000**, *16*, 9147.

(3) Maraval, V.; Laurent, R.; Donnadieu, B.; Mauzac, M.; Caminade, A.-M.; Majoral, J.-P. *J. Am. Chem. Soc.* **2000**, *122*, 2499.
(4) Pan, Y.; Ford, W. T. *Macromolecules* **1999**, *32*, 5468.
(5) Watkins, D. M.; Sayed-Sweet, Y.; Klimash, J. W.; Turro, N. J.; Tomalia, D. A. *Langmuir* **1997**, *13*, 3136.
(6) Mansfield, Marc L. *Polymer* **1994**, *35*, 1827.
(7) Schick, M., *Int. J. Eng. Sci.* **2000**, *38*, 999.
(8) Matsen, M. W.; Bates, F. S. *Macromolecules* **1996**, *29*, 1091.
(9) Vavasour J. D.; Whitmore M. D. *Macromolecules* **1993**, *26*, 7070.
(10) Milner, S. T. *Macromolecules* **1994**, *27*, 2333.
(11) Frischknecht, A.; Fredrickson, G. H. *Macromolecules* **1999**, *32*, 6831.
(12) Edrington, A. C.; et al. *Adv. Mater.* **2001**, *13*, 421.
(13) Subramanian, G.; Manoharan, V. N.; Thorne, J. D.; Pine D. J. *Adv. Mater.* **1999**, *11*, 1261.
(14) Tomalia, D. A.; Hedstrand, D. M.; Ferritto, M. S. *Macromolecules* **1991**, *24*, 1435.
(15) Lescanec, R. L.; Muthukumar, M. *Macromolecules* **1991**, *24*, 4892.
(16) Milner, S. T. *Science* **1991**, *251*, 905 1991.
(17) Pickett, G. T. *Macromolecules* **2001**, *34*, 0000.
(18) Alexander, S. *J. Phys. (Paris)* **1977**, *38*, 983.
(19) de Gennes, P.-G. *J. Phys. (Paris)* **1976**, *36*, 1443.
(20) de Gennes, P.-G.; Hervet, H. *J. Phys. (Paris)* **1983**, *44*, L351.
(21) Lescanec, R. L.; Muthukumar, M. *Macromolecules* **1990**, *23*, 2280.
(22) Mansfield, M. L.; Klushin, L. I. *Macromolecules* **1993**, *26*, 4262.
(23) Boris, D.; Rubinstein, M. *Macromolecules* **1996**, *29*, 7251.
(24) Topp, A.; Bauer, B. J.; Klimash, J. W.; Spindler, R.; Tomalia, D. A.; Amis, E. J. *Macromolecules* **1999**, *32*, 7226.
(25) Semenov, A. N. *Sov. Phys. JTEP* **1985**, *61*, 733.
(26) Milner, S. T.; Witten, T. A.; Cates, M. E. *Macromolecules* **1988**, *21*, 2610.
(27) Ball, R. C.; Marko, J. F.; Milner, S. T.; Witten, T. A. *Macromolecules* **1991**, *24*, 693.
(28) Fleer, G.; Cohen-Stuart, M. A.; Scheutjens, J. M. H. M.; Cosgrove, T. Vincent, B. *Polymers at Interfaces*; Chapman and Hall: London, 1993.
(29) Drolet, F.; Fredrickson, G. H. *Phys. Rev. Lett.* **1999**, *83*, 4317.
(30) Press: W. H.; Teukolsky, S. A.;, Vetterling, W. T.; Flannery, B. P. *Numerical Recipes in C*; Cambridge: Cambridge, England, 1992.

MA011532I